Hindawi Publishing Corporation
ISRN Materials Science
Volume 2013, Article ID 637608, 17 pages
http://dx.doi.org/10.1155/2013/637608

Review Article

Semiconductor Characterization by Scanning Ion Beam Induced Charge (IBIC) Microscopy

Ettore Vittone

Department of Physics, CNISM and NIS Centre of Excellence, University of Torino, Via P. Giuria 1, 10125 Torino, Italy

Correspondence should be addressed to Ettore Vittone; ettore.vittone@to.infn.it

Received 19 September 2012; Accepted 16 October 2012

Academic Editors: Y. Ge, Y. Kusano, V. Ralchenko, and H. Yasuda

The ion beam induced charge (IBIC) technique is a scanning microscopy technique which uses finely focused MeV ion beams as probes to measure and image the transport properties of semiconductor materials and devices. Its success stems from the combination of three main factors: the first is strictly technical and lies in the availability of laboratories and expertise around the world to provide scanning MeV ion beams focused down to submicrometer spots. The second reason stems from the peculiarity of MeV ion interaction with matter, due to the ability to penetrate tens of micrometers with reduced scattering and to excite a high number of free carriers to produce a measurable charge pulse from each incident ion. Last, but not least, is the availability of a robust theoretical model able to extract from the measurements all the parameters for an exhaustive characterization of the semiconductor. This paper is focused on these two latter issues, which are examined by reviewing the current status of IBIC by a comprehensive survey of the theoretical model and remarkable examples of IBIC applications and of ancillary techniques to the study of advanced semiconductor materials and devices.

1. Introduction

A charged particle with energy higher than 10 eV (i.e., charged particulate ionizing radiation) passing through a material deposits energy mainly through Coulomb interactions with the electrons within the absorber atoms [1–3].

If the primary charged particles are electrons, a large fraction of their energy can be lost in a single interaction, and their trajectories within the material are very tortuous because their mass is equal to that of the orbital electrons with which they are interacting.

Also in the case of energetic (MeV) ions, most of their energy is lost in collisions with the atomic electrons; the interactions with the atomic nuclei occur much more rarely.

Therefore, the ion undergoes a huge number of interactions and gradually loses its kinetic energy: the net effect is a gradual decrease of its velocity until the particle is stopped. The range of MeV light ions in matter is mainly determined by the electron stopping power (i.e., the average energy loss of the ion per unit path length) and depends on both the ion and target masses, atomic number, and ion velocity; for MeV light (H or He) ions, it extends to distances of the order of tens of micrometers (an exhaustive review of ion energy loss mechanisms in matter can be found in chapter 2 of [1]).

Moreover, because of the high ion/electron mass ratio, the trajectories of MeV ions undergo few large angle scattering interactions with the sample nuclei owing to their high momentum; accordingly, ion trajectories are nearly straight lines until they are close to the end of their range, where the nuclear stopping cross section becomes no more negligible. Monte Carlo simulators of ion energy loss such as stopping range in matter (SRIM) [4] are readily available for estimating the depthwise energy-loss profile of an MeV ion.

The interaction of the primary ions with the atoms in the material induces the release of energetic electrons (delta rays) with eV to keV energy, that subsequently lose their energy through the interaction with the orbital atomic electrons. In a semiconductor, the overall significant effect is the production of many electron-hole pairs (EHPs).

The net result of such a process is the generation of a plasma volume along the ion track, with a submicrometer radial extension and a characteristic cone shape due to

the fact that, as the ion slows down, delta rays become less energetic, and the generation volume collapses at the end of ion range [5, 6].

According to the semiempirical model of Klein [7], the amount of energy available to create EHPs is largely independent of both the energy and type of the ionizing radiation, and the average energy required to produce one electron-hole pair is of the order of few eV (3.62 eV at 300 K in Si) and is linearly related to the semiconductor bandgap.

In summary, the interaction of a single MeV ion with a semiconductor material generates a high-density volume of free carriers along the ion trajectory, which is nearly a straight line, with a typical energy-loss profile, known as Bragg curve, peaked at the end of the ion range.

Due to the high number of EHPs created, a measurable charge pulse can be extracted from each ion strike and processed by an external circuit, which allows the generation of a histogram of pulse heights (the pulse height spectrum). In case of monoenergetic radiation, the counts are distributed around an average pulse height which is called the peak centroid. The position of the peak centroid is proportional to the measured charge at the electrode; the ratio of such a charge and the charge generated by ionization is the charge collection efficiency (CCE), which is the most important parameter used to characterize electronic devices, in particular semiconductor detectors [2].

The electronic response of a semiconductor to the irradiation of a single MeV ion is a function of the generation profile and of the mechanism of charge-pulse formation: the former depends on ion energy and mass and on the material structure and composition; the latter depends on the electric potential distribution and on the transport properties of free carriers in the material.

As a consequence, if a monochromatic ion probe is provided by an MeV ion accelerator, the measurement of charge pulses provides valuable information on the electronic characteristics of semiconductors. Moreover, these informations are greatly enhanced if the MeV ion beams are focused and raster scanned over the surface of the specimen.

In fact, the knowledge of the ion strike position combined with the almost straight ion trajectory, the large analytical depth, which can be modulated as function of ion energy and mass and the submicrometer radial extent of the charge carrier generation volume, allows the electronic features of semiconductors to be spatially resolved at the micrometer level.

These are, in summary, the main features of the ion beam induced charge (IBIC) microscopy, which has found widespread applications since the early 1990s [8] for the characterization of electronic materials and devices, with considerable research activities carried out in many laboratories, as testified by the numerous papers published in journals as *Nuclear Instruments and Methods in Physics Research* and dedicated sessions in international conferences as the *International Conference on Nuclear Microprobe Technology and Applications* [9].

In the last twenty years, some review papers [10, 11] and textbooks [3] have been published on the experimental setups, measurement protocols, and applications of IBIC to image and analyse the electronic properties of microelectronic devices, dislocations, semiconductor radiation detectors, semi-insulating materials, high power transistors, charge-coupled arrays, solar cells, and light-emitting diodes, in conjunction with single event upset imaging.

This paper focuses on some theoretical aspects, which are needful to provide solid interpretations of IBIC experiments and remarkable examples of electronic characterization of important semiconductor materials.

2. Charge Induction and Signal Formation

As already stated in the previous section, the interaction of an MeV ion with atomic orbital electrons in a semiconductor produces a high density of EHPs along the ion track. The dielectric relaxation time (defined as the product of the resistivity times the dielectric constant) gives an estimate of the time required to recover the neutrality of the material after the free-carrier injection. If the material is in the relaxation regime, that is, if the dielectric relaxation time is much longer than the carrier lifetime, [12], in presence of an electric field, EHPs pairs are swept out of the device without replenishment from contacts. This occurs in wide bandgap materials, that is, insulators as diamond or semi-insulators as SiC, or in the depletion region in p-n or Schottky junction. Under the relaxation regime, the semiconductor behaves as a capacitor, and the presence of charges in the volume where the electric field is not zero leads to the induction of charge at the electrodes.

By virtue of the presence of the electric field, the free carriers drift. In most cases, their velocity is low compared to the velocity of light, so that the magnetic field effects of the moving carriers can be neglected, and the electric field can be regarded as instantaneously propagating. Under these assumptions, the problem can be treated as electrostatics at each moment of charge movement [13, 14]. If the excess charge produced by radiation interactions does not significantly perturb the electric field within the semiconductor, the charge induced at the electrode by the carriers generated by ionization can be calculated through the reciprocal Green's theorem [15].

Methods for calculation have been developed between the years 1930 and 1940 to evaluate the instantaneous value of the current induced by moving charges over its entire time of transit in a vacuum tube [16–18]; the validity of these results was then extended to more general cases in presence of stationary space charge. This theory is then able to model the charge pulse formation in depleted regions of any semiconductor device [19, 20].

Gunn [21] proposed in the year 1964 an expression, deduced under general conditions, for the evaluation of the charges induced upon a system of conductors by the motion of a small charge nearby.

According to the Gunn theorem, the current induced by a moving charge (q) on the ith electrode in a system consisting of multiple electrodes is

$$I_i = -q \cdot \vec{v} \cdot \frac{\partial \vec{E}}{\partial V_i}, \tag{1}$$

where $\vec{v}$ is the velocity vector of the moving charge, and $\partial\vec{E}/\partial V_i$ is the "Gunn's weighting field," which is defined as the derivative of the electric field due to the bias voltage V_i applied at the ith electrode, while the voltage is kept constant on all the other electrodes.

The expression (1) is sufficiently general to be used when space charges of variable magnitude are present and hence applicable to any semiconductor junction, whatever is their polarization state [22, 23].

In order to evaluate the total charge Q_i induced at the ith electrode, it is sufficient to integrate (1) in time, that is,

$$\begin{aligned} Q_i(t) &= \int_0^t I_i\left(t'\right) dt' = -q \cdot \int_{r_I}^{r_F} \frac{\partial \vec{E}}{\partial V_i} \cdot d\vec{\ell} \\ &= q \cdot \left[\left.\frac{\partial \Psi}{\partial V_i}\right|_{r_F} - \left.\frac{\partial \Psi}{\partial V_i}\right|_{r_I} \right], \end{aligned} \tag{2}$$

where r_F and r_I are the charge final and initial positions at time t and 0, respectively.

The induced charge is then simply given by the difference in the Gunn's weighting potential $\partial\Psi/\partial V_i$ between any two positions of the moving charge [24, 25].

The procedure to calculate the charge as a function of time is the following.

(I) The electrostatic potential and electric field distributions have first to be evaluated by solving the relevant Poisson's and continuity equations of electrons and holes, with suitable boundary conditions.

(II) The Gunn's weighting field (GWF) and potential have to be evaluated by differentiating the actual potential Ψ with respect to the potential at the ith electrode.

(III) Finally, the induced charge is evaluated by calculating the GWF at the initial and final points of the carrier trajectory.

The validity of (1) and (2) can be easily extended to the case of a continuous distribution of excess free carriers (electrons or holes) as follows:

$$Q_i(t) = -q \cdot \int_0^t dt' \int_\Omega d^3 r \left\{ x(\vec{r}, t) \cdot \overrightarrow{v}_x(\vec{r}) \cdot \frac{\partial \vec{E}(\vec{r})}{\partial V_i} \right\}, \tag{3}$$

where Ω is the volume of the semiconductor, and x is the excess carrier concentration, whose evolution can be calculated by solving the electron/hole continuity equations [26].

An efficient method, namely, the "adjoint method," to evaluate the induced charge in the whole semiconductor volume was proposed by Prettyman [14, 27] and adopted by other authors [22, 28, 29]. This method is based on the linearization of the continuity equations of electrons and holes; it turns out that (3) is the Green's function of the carrier (electron or hole) continuity equations, assuming a generation term equal to $G_x = \overrightarrow{v}_x(\vec{r}) \cdot (\partial\vec{E}(\vec{r})/\partial V_i)$. As a consequence, the contribution of electrons and holes to the induced charge can be evaluated by solving the adjoint equation of the relevant continuity equations.

The complete map for any point in the semiconductor domain of induced charge is then obtained by solving a unique (for each carrier) partial differential equation by numerical (typically the finite element, FEM) methods. Finally, the knowledge of the induced charge map Q allows the evaluation of the time evolution of the induced charge generated with an arbitrary distribution of noninteracting particles. It is worth underlying that the validity of this approach stems from the superposition principle, which derives from the assumption that the basic differential equations are linear, that is, the excess charge generated does not significantly perturb the electrostatic field within the device. Such assumption holds only if light (H or He) ions are considered, but not, in general, in the case of high carrier injection induced, for example, by heavy ions; the Shockley-Ramo-Gunn approach is then unsuitable to interpret effects as plasma delay or funnelling, occurring when semiconductor devices are irradiated with heavy ions. In these cases, a "technology computer aided design (TCAD) based approach" is usually adopted, which solves the Poisson equation, continuity equations, and transport models self-consistently [30].

An alternative Monte Carlo approach to realistically model the induced charge pulse formation has been recently presented by Olivero et al. [31]. Starting from the evaluation of the Gunn's weighting potential by solving the electrostatic problem by the finite element method, the free carrier trajectories are determined by the random walk method; finally, the induced charge at the sensing electrode is then evaluated by means of (2). The advantage of this method is that it is suitable to simulate problems involving variables following stochastic distributions, as to simulate electronic noise, statistical fluctuations in carrier generation, or randomly distributed recombination centres.

3. Ion Beam Induced Charge Microscopy

IBIC microscopy uses focused MeV light ion (typically H or He) beams in low current mode, that is, using an ion current of the order of fractions of fA corresponding to a count rate of few kHz. Magnetic or electrostatic quadrupole lenses are used to focus the beam; the best reported resolution to date is less than 0.1 μm^2, but an improvement of at least one order of magnitude is expected in the near future [32]. A magnetic scanning system is used to scan the focused beam over the region of interest, which typically extends to area of mm^2.

Unless other microscopy techniques as electron or optical beam induced currents (EBIC [33] and OBIC-LBIC [34], resp.), individual charge pulses, and not continuous variations of charge or currents, produced by the interaction of the ion with the semiconductor sample are measured in IBIC experiments. The current induced at the sensing electrode by the motion of the EHPs generated by a single ion is integrated and amplified by a low-noise electronic chain, digitized and recorded by a data acquisition system along with the corresponding spatial coordinates of the ion probe. Details of the nuclear microprobe components and of the experimental procedure can be found in [3].

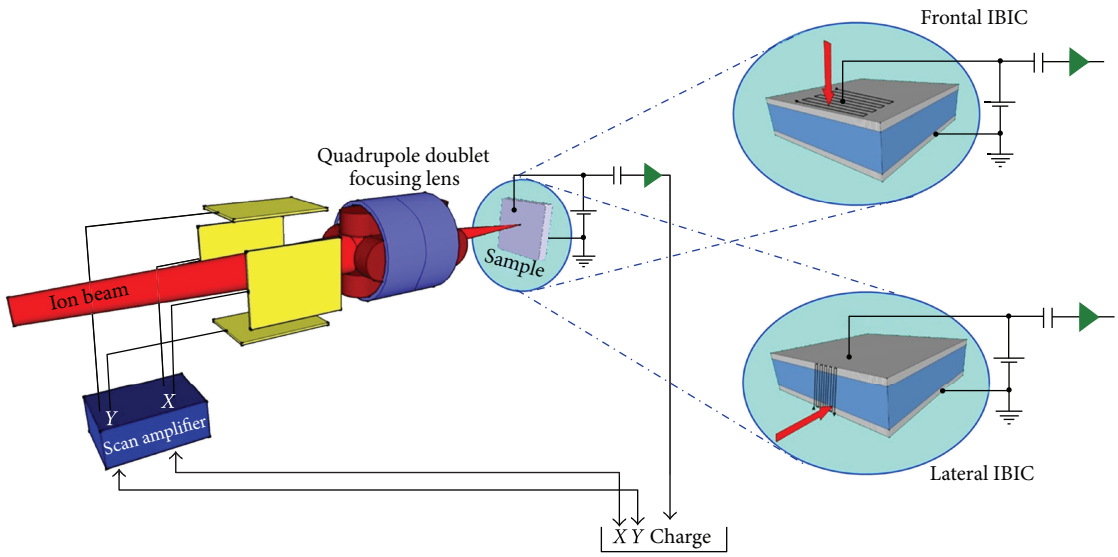

Figure 1: Scheme of the IBIC setup. A MeV ion beam from an accelerator is focused by a quadrupole lens system and scanned over the sample surface using two sets of magnetic or electrostatic plates. The insets on the right sides show the two irradiation geometries: from the top (frontal IBIC) and from the side (lateral IBIC) of the device under analysis. Each incident ion generates a measurable charge pulse, which is amplified and processed by a standard charge sensitive electronic chain. The data acquisition system acquires and stores every event along with the coordinates of the ion.

The induced charge is the usual physical observable imaged as function of the ion strike position. The recent development of waveform digitizers with subnanosecond time resolution enables the study of the time evolution of the induced current. This technique, namely, time- (or transient-) resolved IBIC (TRIBIC), first developed at the Sandia National Laboratories [35], allows the measurement of the carrier transport parameters (mobility and lifetime) by the deconvolution of the transient current pulses; as an example, the measurement of the risetime of the integrated charge pulse as function of the ion strike position and at different applied bias voltages allows electron and hole mobilities to be mapped [36].

IBIC (or TRIBIC) experiments can be performed in two geometrical configurations (Figure 1): frontal IBIC and lateral IBIC.

In frontal IBIC, the ion beam is raster scanned onto the sample electrode; this is the traditional and easier irradiation geometry used to obtain two-dimensional images of the charge collection efficiency [37]. In lateral IBIC, a cleaved semiconductor sample is irradiated from the side, in order to generate carriers at different depths beneath the electrode surfaces. It enables more in-depth studies of the motion of induced charges by profiling the charge collection efficiency as a function of the ion beam position with respect to the sensing electrode [38, 39].

In the following, some significant examples of material characterization, relevant to the semiconductor materials most studied by IBIC, are reviewed. They illustrate the potential of the IBIC technique for the characterization of homogeneous or polycrystalline materials and basic semiconductor devices as metal-semiconductor interfaces, p-n junctions, heterojunction interfaces, and Metal-Oxide-Semiconductor structures.

3.1. Silicon. The first applications of IBIC in the early 1990s were devoted to image device depletion regions through thick metallizations [3, 8, 40] in silicon devices. Since p-n junction behaviour is well known and junction devices fabrication is very reproducible, some experiments have been carried out to validate the theoretical model and to develop suitable algorithms to extract data for the electronic characterization of the material.

A meaningful example of the evolution of the interpretative model of the IBIC experiments can be extracted from lateral IBIC measurements carried out on commercially available silicon p^+-n-n^+ diodes using a low-intensity 5 MeV-proton microbeam [41]. Figure 2 shows the scheme of the experimental setup and the charge collection efficiency (CCE) profiles relevant to pristine and Au contaminated diodes. It is apparent that the charge collection efficiency profiles show broad plateaux with values close to 100%, which widen as the applied bias voltage increases. The region where the electric field is absent shows exponentially decreasing profiles. A simple drift-diffusion model allowed the extraction of the electronic features of the device, which was arbitrary divided in two main regions. The first region is where the electric field is high and the carrier velocity is close to saturation. This means that all the carriers cross the entire depletion region (the region with a nonnull electric field), since the drift time is much shorter than the carrier lifetime. The measurement of the evolution of the CCE plateau width as function of the applied bias voltage allowed the depletion layer width to be estimated and compared with the standard Capacitance-Voltage measurements usually carried out for the determination of the bulk doping profile.

The carrier transport in the second region is dominated by the diffusion mechanism. Charge carriers generated in this region, where no electric field occurs, diffuse towards

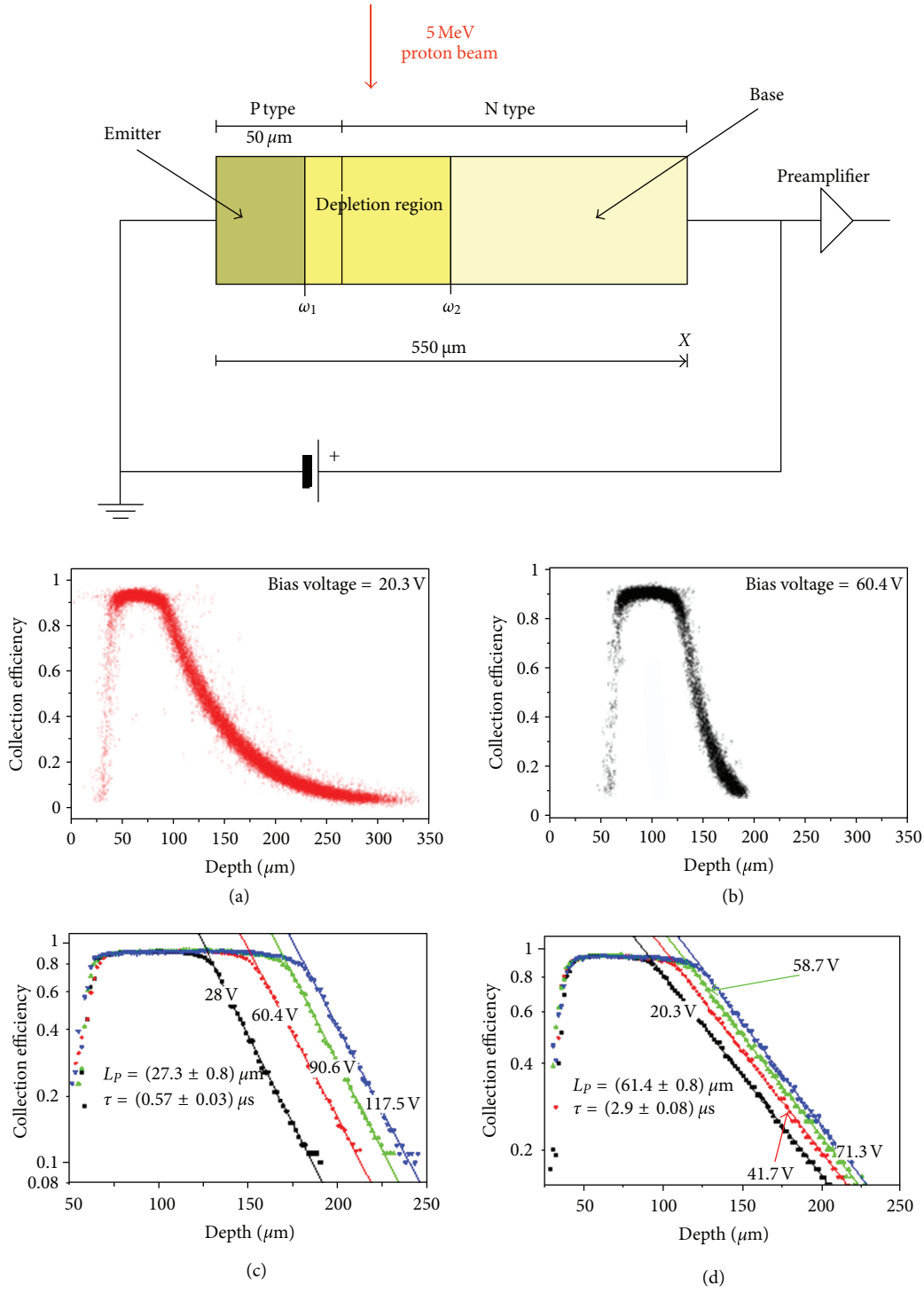

Figure 2: Top: schematics of the experimental set-up. Charge collection efficiency profiles from lateral IBIC experiments on p+-n-n+ silicon diode without (a, d) and with (b, c) Au contamination. (a, b) Lin-lin scale at fixed bias voltage; (d, c) Lin-log scale at different bias voltages. For details, see [41]. L_p = Hole diffusion length, τ = Hole lifetime.

the depletion region, where they are subsequently injected in the depletion region, allowing the induced charge signal to be formed. The estimate of the decay rate allowed the diffusion length of the minority carriers in the bulk of the device to be measured. As an example, Figure 2, elaborated from [41], shows lifetime killing effects induced on the same diode by Au contamination.

Afterwards, a more refined model based on the Shockley-Ramo theorem was implemented for the analysis of diodes with nonconstant doping profiles [42]. However, a

comprehensive model, which did not account for the artificial division in regions with different transport mechanisms, was developed few years later on the basis of the Gunn's theorem [22] and was successfully applied for the interpretation of lateral IBIC experiments [43] and of time resolved IBIC measurements carried out on similar diodes [44].

The importance of diffusion in the formation of the induced charge signal was investigated by Guo et al. [45] by using the "diffusion-time-resolved ion-beam-induced charge collection" (DTRIBICC) technique to measure the average arrival time of the diffused charge, in specially designed stripe-like test junctions using 12 MeV C ion microbeam.

Frontal IBIC was extensively used to characterize high power diodes where, in the design process, the knowledge of the electrical field strength distribution is crucial, in order to optimize the termination structure, for example, the floating ring termination. In these experiments, the long range probing depths of MeV protons were exploited to investigate p-n junctions located tens of micrometers below the surface to achieve sufficiently high breakdown voltages of the order of 10 kV [46, 47].

Silicon-charged particle detectors (as passivated implanted planar silicon, PIPS) produced by diffused-junction or surface barrier technologies have been extensively studied by IBIC technique to evaluate the detector response and its dependence on operating bias and to quantify ion energy loss in the dead layer and loss of the charge collection efficiency due to trapping centres [48].

Similarly, accurate analyses of silicon PIN photodiodes have been carried out because of their widespread applications not only limited to photon detection in the optical region, but now extended to nuclear radiation (X- and gamma-rays, charged particles) detection [49], with spectroscopic performances comparable with dedicated semiconductor detectors and with a more competitive price/quality value.

A remarkable example of IBIC application and a simple but significant interpretation of the experimental results are given by the study of the ion beam induced charge in Metal-Oxide-Semiconductor (MOS) structures, which are one of the main building blocks of microelectronic circuits. When carriers are exposed to heavy high energy ions, the movement of carriers generated by ionization results in a change of the voltage on the electrodes, which can lead to the change of the logical state of the microcircuit (namely, single event upset, SEU). This is what happens, for examples, in microcircuits working in satellites or spacecrafts which are exposed to high energy cosmic radiation [11]. The silicon-on-insulator (SOI) technology was supposed to be less prone to SEU from heavy ion strikes than bulk silicon circuits, since the carriers generated in the active region are only a small fraction of the total charge generated by ionization. However, an unexpected charge collection was observed in SOI deriving from the charges generated below the buried oxide [50] and successively confirmed and analysed in details by IBIC and TRIBIC measurements [51]. The interpretation of these results was first carried out by TCAD simulations [52]; however, an exhaustive explanation of the charge induction in MOS structures has been proposed by Vizkelethy et al. [53], who have developed an analytical model based on the Shockley-Ramo-Gunn theorem for the analysis of the charge induction efficiency dependence on the applied bias voltage for different doping levels and oxide thicknesses.

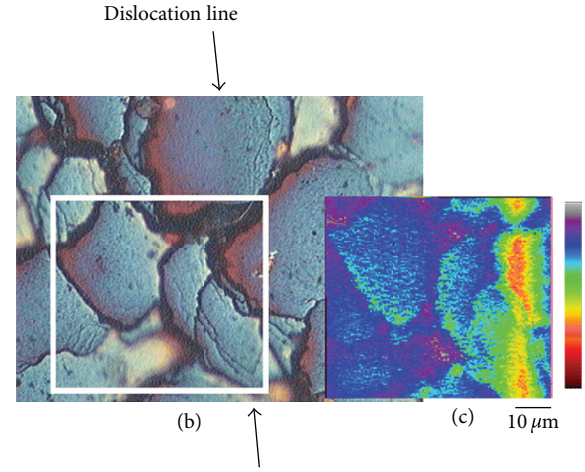

Figure 3: (b) Optical photograph of the solar cells sample, and (c) is the corresponding IBIC image within the white box in (b), which contains a dislocation line. Grey indicates high charge collection efficiency, and red indicates poorer charge collection efficiency. Reprinted from [57] with permission from Elsevier.

Another IBIC/TRIBIC application, related to the aforementioned MOS analysis, was recently carried out by Alves et al. [54] in a MOS Field-Effect Transistor (MOSFET) device. In this study, the electronic signal is not the induced charge at the sensing electrode processed by a charge sensitive preamplifier, as in conventional IBIC. Instead, it is the modulation of the source-drain current produced by the effective change of the gate voltage induced by a single ion strike. Hence, the use of a raster scanning MeV ion beam can provide maps of the device sensitivity to ionization radiation impact, resulting in an optimization of the design of space electronics or in the characterization of microdosimeter architectures.

Grain boundary effects in polycrystalline silicon solar cells have been analysed by IBIC in numerous researches [55–61]. These two-dimensional boundaries behave as recombination and/or trapping centres because they accommodate high concentration of strained Si-Si bonds and dangling bonds and are preferential sites for segregation of impurities. As an example, Figure 3 shows the optical image and the relevant IBIC map of a n^+/p polycrystalline solar cell irradiated with 2 MeV He ions. The inhomogeneity of the IBIC response is clearly due to the presence of strong recombination effects occurring at the grain boundary. However, it is worthwhile to notice that the low-efficiency region indicated by red colour is a dislocation line which could not be clearly observed in optical microscopy.

Donolato et al. [55, 56] have proposed an efficient model based on the diffusion equation to evaluate the charge collection efficiency under the influence at the grain boundaries. Inter- and intra-grain defects have been investigated by Lee and Jamieson [57] performing IBIC experiments at cryogenic temperature. The high sensitivity achieved in this work was

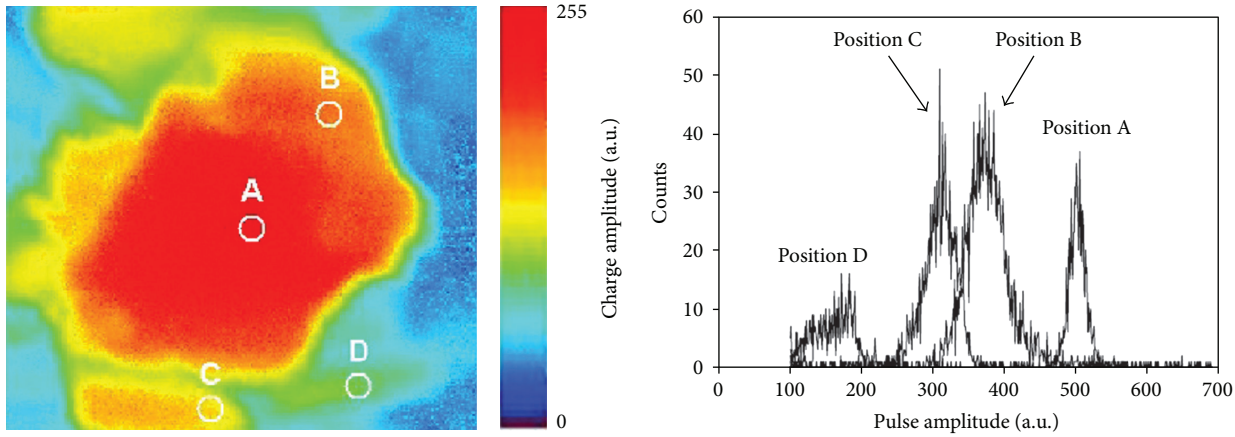

(a) (b)

Figure 4: (a) IBIC image of a single diamond crystallite from the coplanar polycrystalline diamond detector. The image was acquired using a 2 MeV-proton beam and with a bias voltage of 370 V. The colour scale shows charge signal amplitude in arbitrary units. The image size is $150 \times 150\ \mu m^2$. (b) IBIC proton height spectra extracted from region labeled A–D. Reprinted from [71] with permission from Elsevier.

mainly due to the decreasing of the specimen's capacitance, resulting in a remarkable improvement of the signal-to-noise ratio. Moreover, the decrease of the leakage current allowed the measurement of the charge collection efficiency also in reverse and forward bias conditions. Borjanović et al. [58, 59] carried out IBIC experiments on edge-defined film-fed grown (EFG) polycrystalline silicon samples to correlate the charge collection efficiency with oxygen segregated close to structural defects. The correlation of IBIC maps with trace impurity distributions evaluated by means of particle induced X-ray emission (PIXE) is still controversial. Witham et al. [60] observed that in some regions of a polycrystalline silicon solar cell, low IBIC efficiency appeared to be correlated with enhanced concentrations of Fe, Cu, and Ti. However, more recently, Jakob et al. [61] showed that there is no correlation observable between CCE variations at grain boundaries and metallic impurities within the PIXE detection limits of a few ppms.

3.2. Diamond. Diamond has a unique combination of extreme physical, electrical, and optical properties, which make it an ideal material for a variety of advanced applications in science and industry. In particular, its large bandgap (5.5 eV), radiation hardness, optical transparency, large saturated carrier velocities, and low atomic number, make diamond a very attractive candidate for the detection of ionizing radiation in applications as dosimeter as well as in high energy experiments.

Diamond as ionization detector was proposed by Hofstadter in the 1940s [62], and several studies were performed for the characterization of the material and for applications in nuclear physics and dosimetry [63, 64]. However, these detectors found restricted usage due to limitations of natural diamonds, mainly the small size and the uncontrolled material characteristics [65]. The recent availability of synthetic samples, grown under controlled conditions by chemical vapour deposition (CVD) technique, makes possible new opportunities for the fabrication and application of diamond detectors [66].

Since the early 1990s, high purity polycrystalline CVD diamond samples have been available for the fabrication of nuclear detectors. However, the polycrystalline nature of the samples strongly affected the performances of the detector in terms of charge collection efficiency average value and data dispersion [67]. The confirmation that the performances of these diamond detectors were determined by the polycrystalline nature of the material was given by a first IBIC experiment in 1995 [68] and since then, a considerable number of works were devoted to the study by IBIC of charge collection efficiency inhomogeneities in CVD polycrystalline diamond detectors [66, 69–71]. A meaningful example of IBIC image is given in Figure 4, which shows an IBIC image of a large crystallite (about $120 \times 120\ \mu m^2$) in a diamond sample. The central region of the crystallite clearly shows a uniform area of maximum pulse height, whereas the edges of the crystallite are marked by a sharp drop in signal amplitude corresponding to boundary regions where the deposited charge has a very short drift length. A model of charge trapping/recombination phenomena was proposed by Milazzo and Mainwood [72]. An efficient method to mitigate the effects of grain boundaries was proposed by Hearne et al. [73], who showed that the charge collection efficiency of polycrystalline CVD diamond detectors increases with increasing temperature. When this trapped charge is released by heating the detector during the collection of induced charge, the local electric field becomes stronger and more uniform causing the charge collection efficiency to increase (Figure 5).

Other IBIC analyses indicated that light illumination contributes to avoid polarization effects (i.e., the dose-dependent decrease of CCE due to the capture of carriers by deep traps and the subsequent buildup of space charge within the material) and to improve diamond nuclear detector performances and response uniformity [74]. As an example, Figure 6 shows

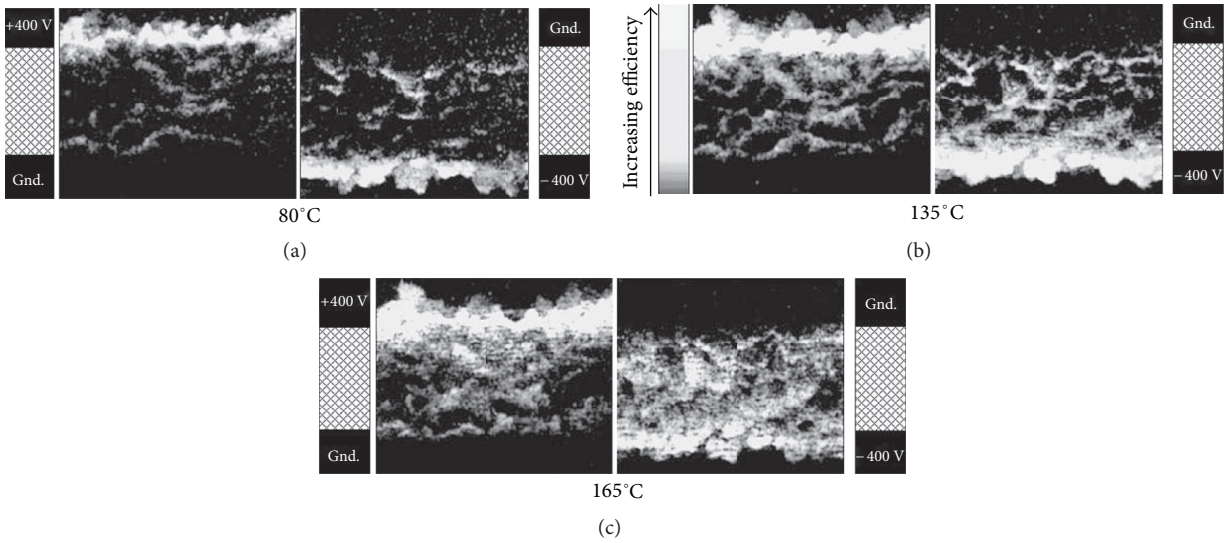

FIGURE 5: Ion beam induced charge maps using a scanned 2 MeV He^+ microprobe collection in CVD diamond at various temperatures. The location of the electrodes is shown. Note that the charge collection efficiency is always highest near to the anode. Reprinted with permission from [73]. Copyright 2004, American Institute of Physics.

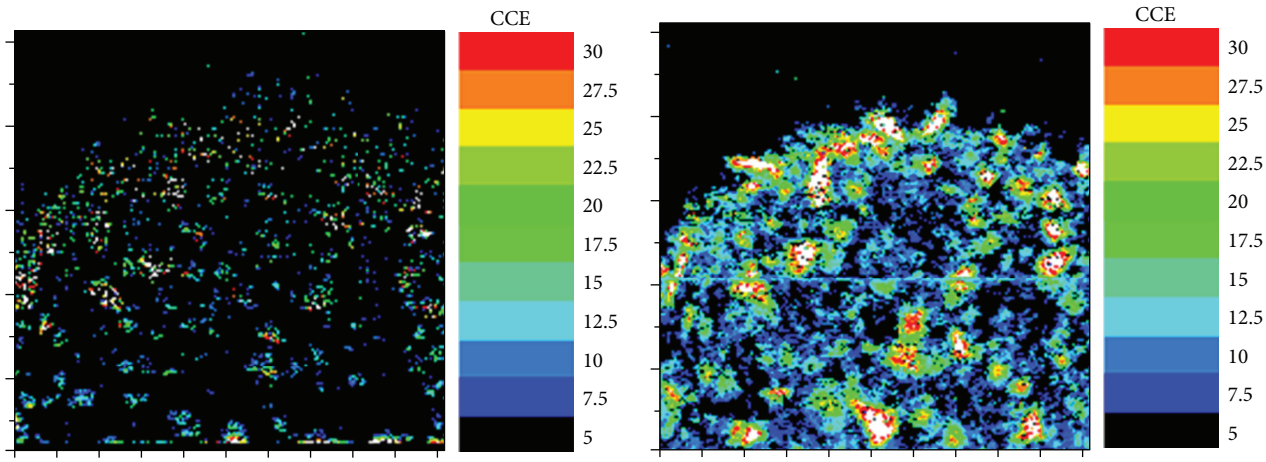

FIGURE 6: IBIC maps (using 2 MeV H^+ ion microbeam) of a polycrystalline CVD diamond detector in dark conditions (b) and under blue (450 nm) light illumination (a). The image size is $1500 \times 1500\ \mu m^2$. For details, see [66, 74].

the evolution of the IBIC maps of a polycrystalline diamond detector from dark to illumination (blue light) conditions.

In order to correlate induced charge maps with the distribution of radiative as well as nonradiative recombination centres across large areas of a CVD diamond film, maps of luminescence induced by ion beams (IBIL technique) were simultaneously acquired along with IBIC maps [75, 76].

The development of the CVD techniques in recent years led to the synthesis of single crystal diamond detectors with performances similar to or even better than performances of natural gems [77]. For these samples, the response is uniform over the whole active detector area, and 100% CCE can be achieved at electric field strengths $> 0.4\ V \cdot \mu m^{-1}$ [78–80].

The absence of grain boundaries allowed the measurements of the effects of structural imperfections and impurities on the charge collection efficiency of CVD single crystal diamond samples. This was successfully accomplished by Lohstroh et al. [81]. In that work, authors clearly correlate regions of reduced CCE with the presence of nitrogen and dislocations evidenced by photoluminescence mapping, which act as efficient electron—hole recombination centres.

IBIC has provided valuable insights not only for the development of diamond detectors as trackers in high energy physics experiments [82], but also in the field of dosimetry. In fact, its unique properties, such as chemical inertness, biocompatibility, radiation hardness, and, above all, its tissue

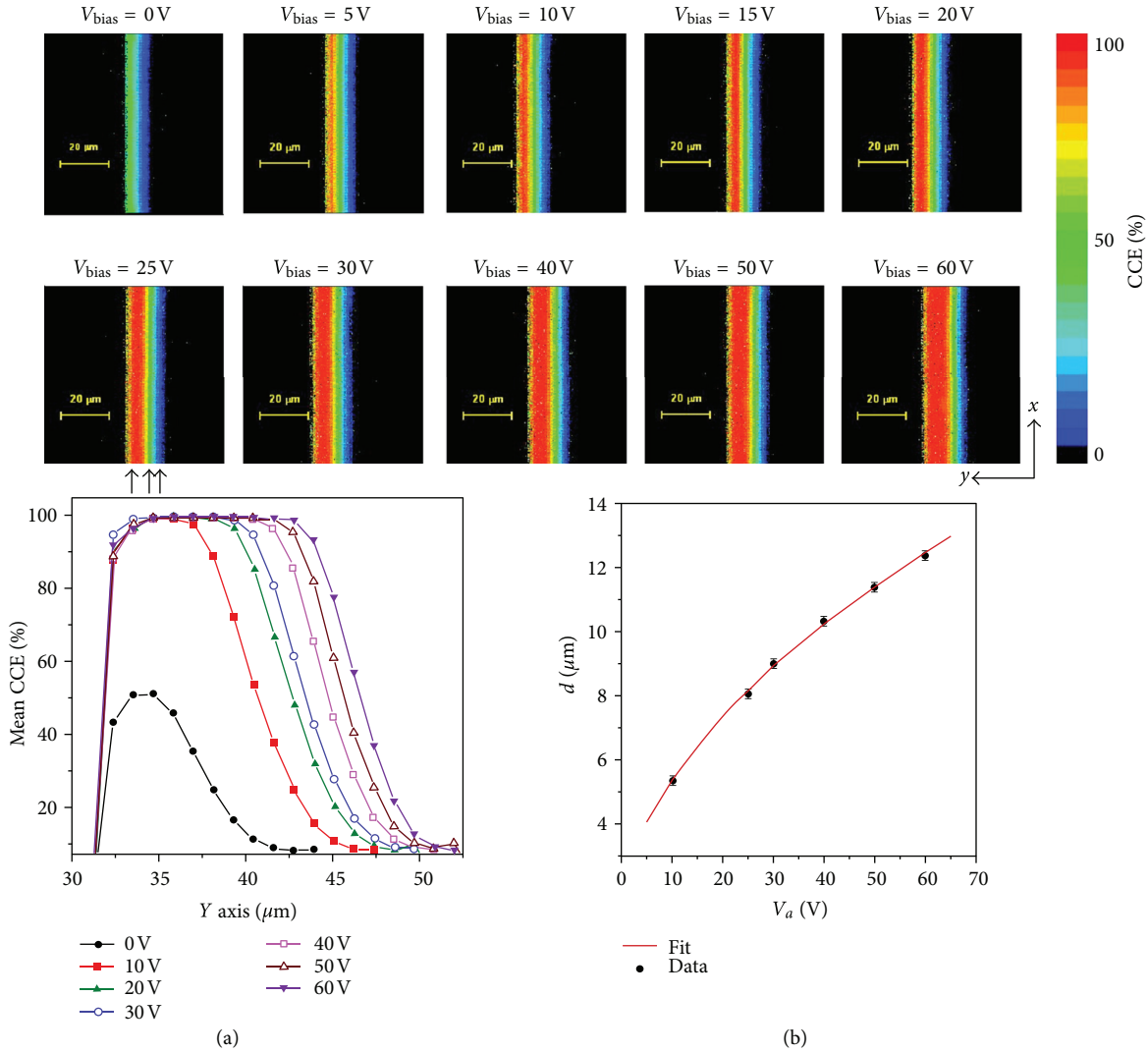

FIGURE 7: Top: lateral IBIC maps relevant to different bias voltages: Schottky contact is on the left side; ohmic contact on the right side. (a) CCE profiles at different bias voltages. (b) Plot of the extension of the depletion region as evaluated from the IBIC maps as a function of applied bias voltage. Reprinted from [83] with permission from John Wiley and Sons.

equivalence, make diamond more suitable than any other solid-state dosimeter [66].

A recent example of IBIC application for the characterization of single crystal diamond dosimeter is given by lateral IBIC experiments carried out to investigate a homoepitaxial diamond Schottky diode detector [83]. Figure 7 shows the evolution of IBIC maps as function of the applied bias. As already observed in the case of Si p-n junction diode, the whole charge generated in the depletion region is collected; by fitting the extension of the depletion region as function of the applied bias voltage, the built-in potential and hence the average doping concentration were estimated, resulting in an excellent agreement with other electrical measurements. In the neutral region, an exponential-like behaviour of the CCE can be observed, whose logarithmic slope is related to the minority carrier diffusion length.

3.3. Silicon Carbide. Silicon carbide (SiC) exists in many different polytypes which differ in the stacking of double layers of Si and C atoms; these differences affect all electronic and optical properties of the crystal. The most interesting SiC polytypes for applications in electronics are 4H and 6H, which are regarded as optimal candidates for high-power and high-frequency devices because of their excellent physical properties such as wide bandgap, high saturation velocity of electrons, high breakdown field, high thermal conductivity, and radiation hardness, similar to diamond [84].

Since the turn of the last decade, SiC p-n and Schottky diodes were studied by IBIC/TRIBIC techniques in order to evaluate their electronic characteristics and to measure the average energy per electron/hole pair generation [85, 86].

An excellent example of the potential of IBIC to visualize the distribution of defects throughout the whole active

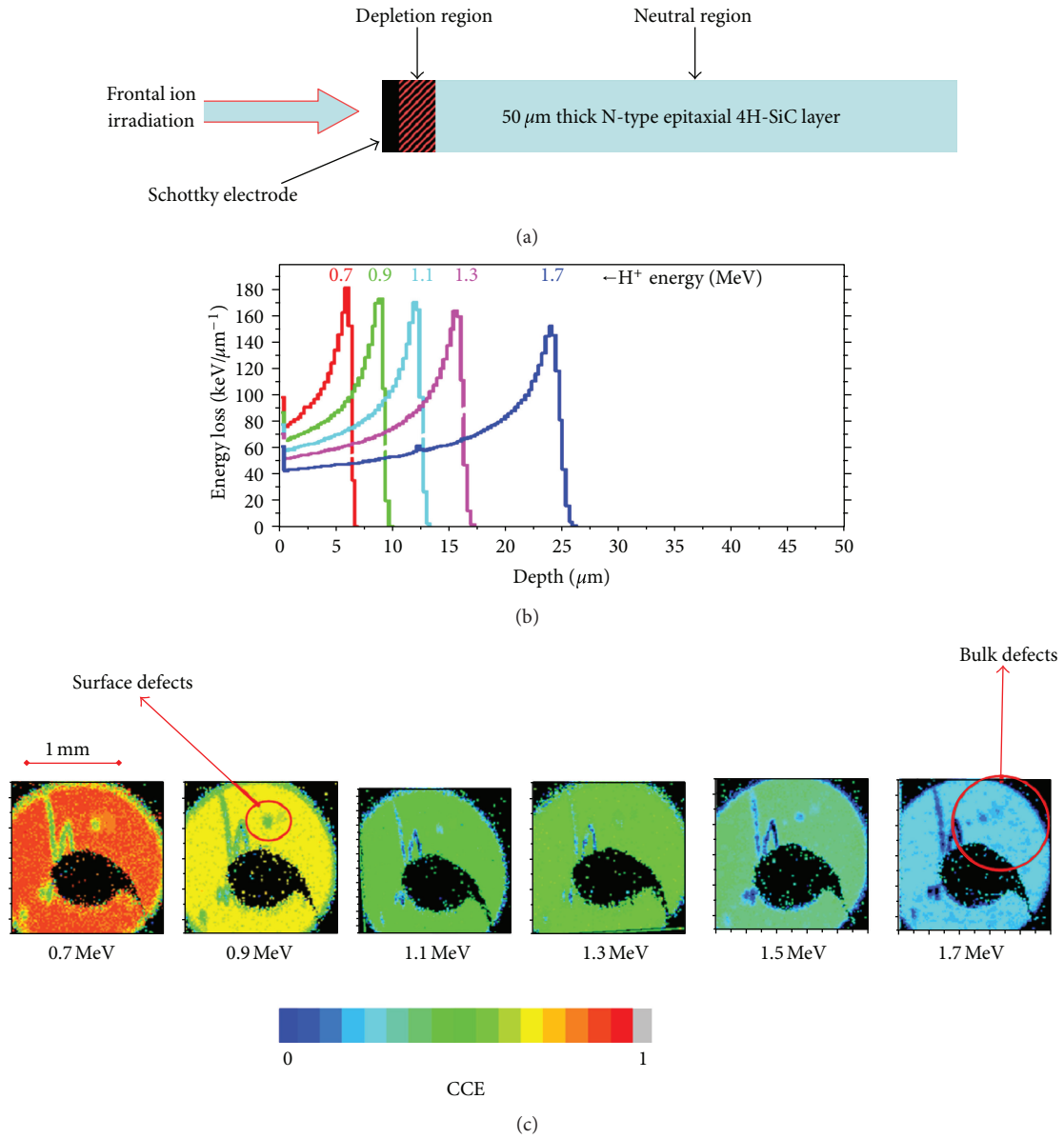

Figure 8: (a) Scheme of the ion irradiation geometry of a 4H-SiC Schottky diode; (b) Ionization curves relevant to 0.7, 0.9, 1.1, and 1.9 MeV H^+ ions in 4H-SiC; (c) charge collection efficiency maps. For details, see [87].

volume was given by Jakšić et al. [87]. In this paper, a 4H-SiC Schottky diode was analysed by using proton microbeams at different energies in order to probe different depth of the epitaxial layer (50 μm thick). The Bragg curves relevant to the different ion energies are shown in Figure 8. The CCE map relevant to the lowest proton energy (0.7 MeV) makes evident the presence of a scratch on the top electrode or shallow defects, since the probing depth is limited to few micrometers. More pronounced inhomogeneities, probably due to the substrate-epitaxial layer interface, are visible in IBIC images with higher proton energies where most of the ion energy loss occurs deeper in the diffusion region.

A different approach [88] to modulate the probing depth of the ion beam consists in the CCE measurement as function of the ion beam angle of incidence (see Figure 9), which allows the minority carriers diffusion length, the energy loss in the dead layer, and the depletion layer width to be measured. In comparison with the aforementioned method [87], it offers the advantage of being much simpler to implement experimentally, it uses a simpler fitting algorithm to extract the physical parameter (e.g., diffusion length), and it is less sensitive to plasma effects due to the increasing carrier density occurring when the Bragg's peak relevant to low energy protons is used.

Another interesting example of IBIC application to study the electronic features of SiC devices and their robustness against ion irradiation has been given by Lee et al. [89], who studied the quality of the silicon dioxide in a MOS

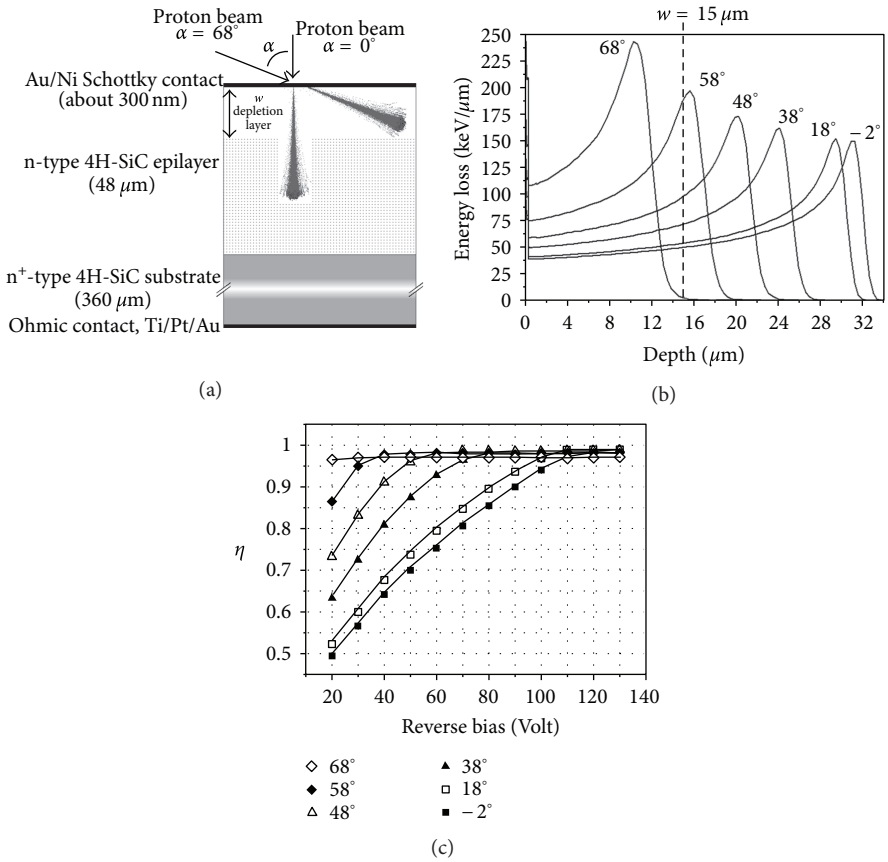

Figure 9: (a) Scheme of the experimental setup for angle-resolved IBIC experiment on a 4H-SiC Schottky diode. (b) Bragg's curves relevant to the ionisation energy profiles of 2 MeV protons incident at different angles in 4H-SiC as evaluated by the SRIM2003 computer code. (c) Charge collection efficiency as function of reverse bias voltage at different angle of incidence; the continuous lines are the theoretical curves from the diffusion-drift model. Reprinted from [88] with permission from Elsevier.

6H-SiC p-type diode. CCE maps evidenced the progressive degradation of the IBIC signals as function of the ion fluence, up to the rupture of the oxide layer induced by the strong electric field occurring between charged traps at the SiO_2/SiC interface and within the oxide filled with electron/hole pairs generated by the scanning 2 MeV He^+ microbeam.

To qualify the native trap in a 4H-SiC Schottky diodes, IBIC measurements of the diffusion length of minority carriers were carried out in the temperature range of 120–380 K [90]. The analysis of this experiment was carried out adopting the Shockley-Read-Hall model for recombination-generation of electron-hole pairs; the resulting trap levels in the gap were in excellent agreement with previous data obtained from deep level transient spectroscopy (DLTS).

Finally, it is worth mentioning that IBIC analysis of 4H-SiC diodes with coplanar-interdigitated Schottky electrode has been recently reported to validate the theoretical framework based on the Shockley-Ramo-Gunn theorem and the relevant computational algorithm for mapping charge pulses generated within the whole detector volume; these studies provided direct evidence of the important role played by diffusion in the charge collection process and in the definition of the active areas in pixellated electrode structures [25].

3.4. Other Wide Bandgap Semiconductors. Cadmium telluride (CdTe) and cadmium zinc telluride (CZT) have received significant attention for the fabrication of X- and gamma-ray detectors.

With respect to Si, they offer two main advantages. Since the cross section for photoelectric effect scales approximately as $Z^{4.5}$ [2], their high atomic numbers ($Z_{Cd} = 48$, $Z_{Zn} = 30$ and $Z_{Te} = 52$) enhance the absorption of high energy photons in relatively small volumes; moreover, their relatively large bandgap energy (around 1.5 eV) and high intrinsic resistivity (>10^9 Ω cm) make these materials attractive for the development of room temperature detectors for medical and technological applications [91].

However, there are specific features which limit the energy resolution of CdTe or CZT detectors.

Technological issues are related to the spatial nonuniformity of the CCE due to the formation of extended defects (as Te inclusions) in high-resistivity crystals [92] and to the development of a reliable method to metalize the surface for the realization of efficient contacts [93].

IBIC analyses have given remarkable contributions to correlate these effects with the performances of detectors; numerous charge collection efficiency maps have been

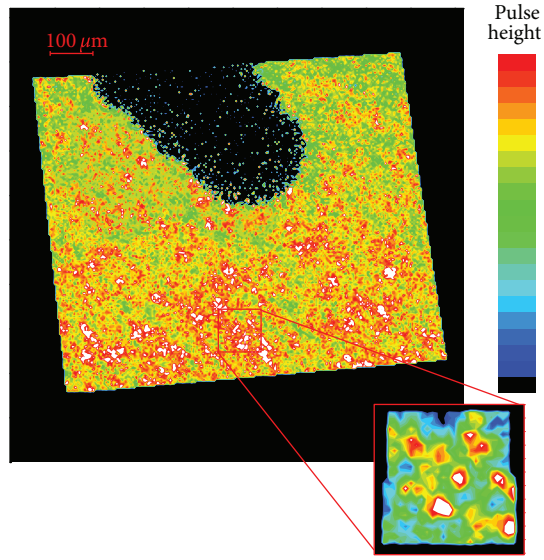

Figure 10: IBIC map of the CdTe/CdS polycrystalline solar cell. The inset show a $100 \times 100\ \mu m^2$ zoom of the map. See [101] for details.

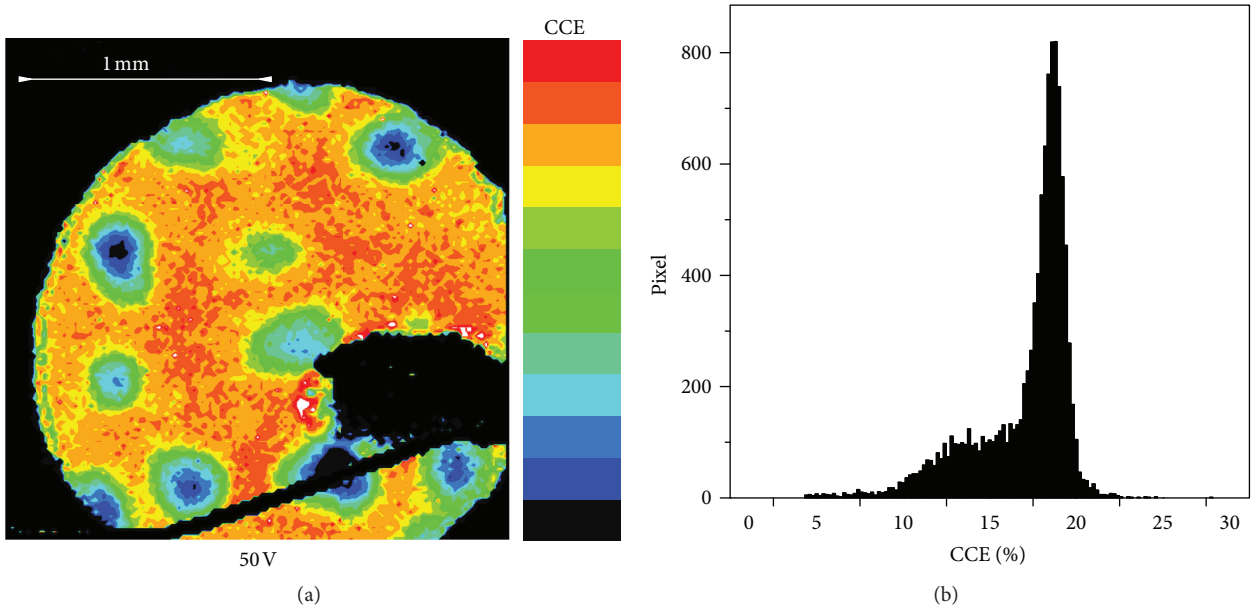

Figure 11: (a) IBIC map of a GaAs Schottky diode obtained using a 2 MeV H^+ microbeam; the reverse applied bias was 50 V. (b) The relevant pulse height spectrum. See [105] for details.

acquired on different materials evidencing the reduction of carrier lifetime in the material close to the inclusions and the nonuniform profile of the electric field profile [94]. These analyses where used to realistically simulate gamma-ray spectral response of CdTe nuclear detectors using Monte Carlo computer codes [95].

Moreover, both CdTe and CZT show an intrinsic limit in energy resolution due to the low hole mobility, resulting in hole drift lengths much shorter than those of electrons. This fact is responsible for the incomplete charge collection in thick detectors required for high-energy gamma-ray detection and, consequently, long tails in the measured spectra. This phenomenon was systematically investigated by several groups in time-resolved IBIC experiments able of event-by-event pulse digitization and acquisition [36, 96] even at different temperature [97, 98]. The different role played by electrons and holes for the charge induction has been clearly evidenced in terms of quantitative mobility lifetime maps and profiles acquired in real time under different polarization conditions.

Polycrystalline CdTe is one of the most important materials for industrial mass production of thin film solar cells: it has the great advantage of being much easier to produce in comparison to crystalline silicon solar cells, and its bandgap

is very close to the theoretical maximum of photovoltaic conversion efficiency of solar energy [99]. As for diamond, IBIC analyses have evidenced that the inhomogeneous nature of polycrystalline CdTe samples strongly affect its electronic transport properties [100].

A finite CdS/CdTe thin solar cell has been recently analysed by IBIC using 3150 keV He ion beams extracted in air and focused onto the back electrode. As an example, Figure 10 shows an IBIC map of a CdTe/CdS solar cell working in photovoltaic mode: pulses generated in regions close to grain boundaries are lower than signals generated within the grains, over a width of a few micrometers [101].

Gallium Arsenide Schottky diodes were among the very first semiconductor devices analysed by IBIC to improve their resistance against single event upsets [102, 103]. Therefore, a systematic IBIC analysis was carried out on Schottky diodes fabricated on semi-insulating GaAs substrates in order to correlate the CCE uniformity with the energy resolution of the device [104]. Figure 11 shows an IBIC map of a GaAs Schottky diode with a reverse bias voltage of 50 V obtained using 2 MeV H^+ ions [105]. The CCE spectrum shows a long tail, which is due to the presence of two spatially distinct "electronic phases" as evidenced by the IBIC map, in which the charge collection is different and which are the responsible for the poor spectral resolution of such a detector at low bias voltages.

Such electronic "phases" show different behaviours as a function of the applied bias voltage, which is likely due to the different electric field dependence on the relevant capture cross sections of the trapping centres for both charge carriers. This interpretation has been subsequently reinforced by lateral IBIC experiments, which evidence the formation of a Mott-like barrier at high electric field due to the electric-field-enhanced capture cross section of electrons from deep donor levels [106].

4. Conclusions

IBIC is a powerful experimental technique for gaining an understanding of the transport mechanisms in semiconductor/insulating materials. Since the earliest works, many laboratories equipped with microfocused MeV ion beams have carried out IBIC experiments for the characterization of basic devices as Schottky, p-n, or MOS diodes as well as of dosimeters, particle detectors, or LEDs [107]. The reason of the widespread use of this technique resides in the availability of tens of high energy microprobes around the world, the widespread expertise on handling and processing charge pulses, commonly used in nuclear spectroscopy, and the possibility of a synergetic coupling with other ion beam analytical (IBA) techniques such as PIXE, IBIL, and scanning ion transmission microscopy (STIM) [108].

The power of IBIC stems from the high sensitivity of the induced charge pulses to electric field, carrier lifetime and mobility, the potential of mapping the charge collection efficiency at the submicrometer scale, and the availability of a robust theoretical framework, suitable algorithms and simulation models, which are capable to extract from the measurements many of the parameters required for a comprehensive characterization of the device under study.

Besides the traditional application of IBIC for the analysis of semiconductor materials and basic device, which have been reviewed in this paper, at present, its use has been extensively adopted to study soft or hard errors occurring in integrated circuits caused by heavy ions [10, 11, 29] and to analyse radiation-induced defects in semiconductors and insulators. In this latter respect, the use of MeV ion microbeams offers the advantage both to damage selected regions and to monitor the radiation-induced defects. An extended literature is available on this subject [1, 10, 11, 80, 101]. A recent paper of Pastuović et al. [109] has proposed an experimental methodology supported with a strong theoretical framework to study the effects of radiation damage in different semiconductors. This protocol is now an object of study from an internationally coordinated project [110] aimed to improve the understanding of how radiation-induced defects form in semiconductors and insulators and how the performances of electronic devices degrade in extreme and harsh radiation environments.

In the field of defect engineering in semiconductors, it is worthwhile to mention the realization of a position-sensitive detector based on the measurement of the CCE degradation in a region with constant damage gradient in Si photodiodes [111].

The potential of IBIC to investigate in depth the electronic features of devices is prospected to provide valuable information for the characterization of novel three-dimensional topologies of radiation detectors. The main advantage of this approach is that the carriers have to travel short drift distances in the bulk of the detector, resulting in fast response, enhanced detection efficiency, and high radiation hardness; and, consequently, promising applications appear feasible in the fields of X-ray medical imaging or particle tracking in high energy experiments [112, 113]. A remarkable example of such applications was given by Olivero et al. [114], who performed IBIC experiments to characterize the charge collection efficiency in a monocrystalline diamond detector with buried microelectrodes fabricated by deep ion beam lithography.

In the near future, it is expected that IBIC gains increasing interest for the measurement of the ion strike location in multielectrode devices. Examples include the development of single-atom deterministic doping techniques, which are now emerging [115] for potential applications in solid-state quantum information processing devices. For such purposes, the evaluation of the induced charge shared between the electrodes could be used for the measurement of the ion strike location to submicron precision. The achievement of this goal requires accurate analysis of the induced charge pulse formation mechanism and a suitable investigation of the main physical phenomena influencing the measurement [116].

References

[1] Y. Wang and M. Nastasi, Eds., *Handbook of Modern Ion Beam Materials Analysis*, Materials Research Society, Warrendale, Pennsylvania, 2nd edition, 2009.

[2] G. F. Knoll, *Radiation Detection and Measurements*, John Wiley & Sons, New York, NY, USA, 3rd edition, 2000.

[3] M. B. H. Breese, D. N. Jamieson, and P. J. C. King, *Materials Analysis using a Nuclear Microprobe*, John Wiley & Sons, 1996.

[4] J. F. Ziegler, M. D. Ziegler, and J. P. Biersack, "SRIM—the stopping and range of ions in matter," *Nuclear Instruments and Methods in Physics Research B*, vol. 268, no. 11-12, pp. 1818–1823, 2010.

[5] J. S. Laird, C. Jagadish, D. N. Jamieson, and G. J. F. Legge, "Scanning ion deep level transient spectroscopy: I. Theory," *Journal of Physics D*, vol. 39, pp. 1342–1351, 2006.

[6] E. J. Kobetich and R. Katz, "Energy deposition by electron beams and δ rays," *Physical Review*, vol. 170, no. 2, pp. 391–396, 1968.

[7] C. A. Klein, "Bandgap dependence and related features of radiation ionization energies in semiconductors," *Journal of Applied Physics*, vol. 39, no. 4, pp. 2029–2038, 1968.

[8] M. B. H. Breese, P. J. C. King, G. W. Grime, and F. Watt, "Microcircuit imaging using an ion-beam-induced charge," *Journal of Applied Physics*, vol. 72, no. 6, pp. 2097–2104, 1992.

[9] B. Tilman, T. Reinert, and D. Spemann, "Editorial of the 2th International Conference of Nuclear Microprobe Technology and Applications (ICNMTA2010)," *Nuclear Instruments and Methods in Physics Research B*, vol. 269, no. 20, pp. 5–6, 2011.

[10] M. B. H. Breese, "A review of ion beam induced charge microscopy for integrated circuit analysis," *Materials Science and Engineering B*, vol. 42, no. 1–3, pp. 67–76, 1996.

[11] M. B. H. Breese, E. Vittone, G. Vizkelethy, and P. J. Sellin, "A review of ion beam induced charge microscopy," *Nuclear Instruments and Methods in Physics Research B*, vol. 264, no. 2, pp. 345–360, 2007.

[12] G. H. Doehler and H. Heyszenau, "Conduction in the relaxation regime," *Physical Review B*, vol. 12, pp. 641–649, 1975.

[13] Z. He, "Review of the Shockley-Ramo theorem and its application in semiconductor gamma-ray detectors," *Nuclear Instruments and Methods in Physics Research A*, vol. 463, pp. 250–267, 2001.

[14] T. H. Prettyman, "Theoretical framework for mapping pulse shapes in semiconductor radiation detectors," *Nuclear Instruments and Methods in Physics Research A*, vol. 428, no. 1, pp. 72–80, 1999.

[15] J. D. Jackson, *Classical Electrodynamics*, John Wiley & Sons, 3rd edition, 1998.

[16] W. Shockley, "Currents to conductors induced by a moving point charge," *Journal of Applied Physics*, vol. 9, no. 10, pp. 635–636, 1938.

[17] S. Ramo, "Currents induced by electron motion," *Proceedings of the IRE*, vol. 27, pp. 584–585, 1939.

[18] C. K. Jen, "On the induced current and energy balance in electronics," *Proceedings of the IRE*, pp. 345–349, 1941.

[19] G. Cavalleri, E. Gatti, G. Fabri, and V. Svelto, "Extension of Ramo's theorem as applied to induced charge in semiconductor detectors," *Nuclear Instruments and Methods in Physics Research*, vol. 92, no. 1, pp. 137–140, 1971.

[20] E. Vittone, F. Fizzotti, A. Lo Giudice, C. Paolini, and C. Manfredotti, "Theory of ion beam induced charge collection in detectors based on the extended Shockley-Ramo theorem," *Nuclear Instruments and Methods in Physics Research B*, vol. 161, no. 1–4, pp. 446–451, 2000.

[21] J. B. Gunn, "A general expression for electrostatic induction and its application to semiconductor devices," *Solid State Electronics*, vol. 7, no. 10, pp. 739–742, 1964.

[22] E. Vittone, "Theory of ion beam induced charge measurement in semiconductor devices based on the Gunn's theorem," *Nuclear Instruments and Methods in Physics Research B*, vol. 219-220, no. 1–4, pp. 1043–1050, 2004.

[23] L. A. Hamel and M. Julien, "Generalized demonstration of Ramo's theorem with space charge and polarization effects," *Nuclear Instruments and Methods in Physics Research A*, vol. 597, pp. 207–211, 2011.

[24] V. Radeka, "Low-noise techniques in detectors," *Annual Review of Nuclear and Particle Science*, vol. 38, pp. 217–277, 1988.

[25] E. Vittone, Z. Pastuović, P. Olivero et al., "Semiconductor characterization by scanning ion beam induced charge (IBIC) microscopy," *Nuclear Instruments and Methods in Physics Research B*, vol. 266, pp. 1312–1318, 2008.

[26] S. Selberherr, *Analysis and Simulation of Semiconductor Devices*, Springer, Vienna, Austria, 1984.

[27] T. H. Prettyman, "Method for mapping charge pulses in semiconductor radiation detectors," *Nuclear Instruments and Methods in Physics Research A*, vol. 422, no. 1–3, pp. 232–237, 1999.

[28] G. Vizkelethy, "Simulation of ion Beam induced current in radiation detectors and microelectronic devices," Sandia National Laboratories Report SAND20096757.

[29] G. Vizkelethy, "Simulation of ion beam induced current in radiation detectors and microelectronic devices," *Nuclear Instruments and Methods in Physics Research B*, vol. 269, pp. 2330–2335, 2011.

[30] J. Laird, T. Hirao, S. Onoda, and T. Kamiya, "The role of high-injection effects on the transient ion beam induced current response of high-speed photodetectors," *Nuclear Instruments and Methods in Physics Research B*, vol. 219-220, pp. 1015–1021, 2004.

[31] P. Olivero, J. Forneris, P. Gamarra et al., "Monte Carlo analysis of a lateral IBIC experiment on a 4H-SiC Schottky diode," *Nuclear Instruments and Methods in Physics Research B*, vol. 269, pp. 2350–2354, 2011.

[32] J. A. van Kan, P. Malar, and A. B. de Vera, "The second generation Singapore high resolution proton beam writing facility," *Review of Scientific Instruments*, vol. 83, pp. 902–905, 2012.

[33] H. J. Leamy, "Charge collection scanning electron microscopy," *Journal of Applied Physics*, vol. 53, no. 6, pp. R51–R80, 1982.

[34] J. Domaradzki and D. Kaczmarek, "Optical beam injection methods as a tool for analysis of semiconductor structures," *Optica Applicata*, vol. 35, no. 1, pp. 129–137, 2005.

[35] H. Schöne, D. S. Walsh, F. W. Sexton et al., "Time-resolved ion beam induced charge collection (TRIBICC) in microelectronics," *Nuclear Instruments and Methods in Physics Research B*, vol. 158, no. 1, pp. 424–431, 1999.

[36] P. J. Sellin, A. Lohstroh, A. Simon, and M. B. H. Breese, "Digital IBIC-new spectroscopic modalities for ion-beam-induced charge imaging," *Nuclear Instruments and Methods in Physics Research A*, vol. 521, pp. 600–607, 2004.

[37] C. Manfredotti, F. Fizzotti, E. Vittone et al., "IBIC investigations on CVD diamond," *Nuclear Instruments and Methods in Physics Research B*, vol. 100, no. 1, pp. 133–140, 1995.

[38] E. Vittone, F. Fizzotti, A. Lo Giudice, P. Polesello, and C. Manfredotti, "Simulation of a CdTe gamma ray detector based on collection efficiency profiles as determined by lateral IBIC," *Nuclear Instruments and Methods in Physics Research A*, vol. 428, no. 1, pp. 81–87, 1999.

[39] C. Manfredotti, F. Fizzotti, P. Polesello et al., "Scanning Ion Beam Microscopy: a new tool for mapping the transport properties of semiconductors and insulators," in *Proceedings of the CP392, Application of Accelerators in Research and Industry*, J. L. Duggan and I. L. Morgan, Eds., pp. 705–708, AIP Press, New York, NY, USA, 1997.

[40] M. B. H. Breese, G. W. Grime, and F. Watt, "The generation and applications of ion beam induced charge images," *Nuclear Instruments and Methods in Physics Research B*, vol. 77, no. 1–4, pp. 301–311, 1993.

[41] E. Vittone, F. Fizzotti, E. Gargioni et al., "Evaluation of the diffusion length in silicon diodes by means of the lateral IBIC technique," *Nuclear Instruments and Methods in Physics Research B*, vol. 158, no. 1, pp. 476–480, 1999.

[42] E. Vittone, C. Manfredotti, F. Fizzotti et al., "Measurements of charge collection profiles in virgin and strongly irradiated silicon diodes by means of the micro-IBICC technique," *Nuclear Instruments and Methods in Physics Research A*, vol. 476, no. 3, pp. 607–613, 2002.

[43] F. Fizzotti, E. Colombo, A. Lo Giudice et al., "Measurement of charge collection profiles in irradiated silicon diodes by lateral IBIC technique," *Nuclear Instruments and Methods in Physics Research B*, vol. 260, no. 1, pp. 259–263, 2007.

[44] C. Manfredotti, F. Fizzotti, A. Lo Giudice et al., "Time-resolved ion beam-induced charge collection measurement of minority carrier lifetime in semiconductor power devices by using Gunn's theorem," *Materials Science and Engineering B*, vol. 102, no. 1–3, pp. 193–197, 2003.

[45] B. N. Guo, M. El Bouanani, S. N. Renfrow et al., "Diffusion-time-resolved ion-beam-induced charge collection from stripe-like test junctions induced by heavy-ion microbeams," *Nuclear Instruments and Methods in Physics Research B*, vol. 181, no. 1–4, pp. 315–319, 2001.

[46] M. Zmeck, L. J. Balk, T. Osipowicz et al., "Ion beam induced charge microscopy studies of power diodes," *Journal of Physics Condensed Matter*, vol. 16, no. 2, pp. S57–S66, 2004.

[47] T. Osipowicz, M. Zmeck, F. Watt et al., "IBIC analysis of high-power devices," *Nuclear Instruments and Methods in Physics Research B*, vol. 181, no. 1–4, pp. 311–314, 2001.

[48] C. Yang, D. N. Jamieson, S. M. Hearne et al., "Ion-beam-induced-charge characterisation of particle detectors," *Nuclear Instruments and Methods in Physics Research B*, vol. 190, no. 1–4, pp. 212–216, 2002.

[49] A. Simon and G. Kalinka, "Investigation of charge collection in a silicon PIN photodiode," *Nuclear Instruments and Methods in Physics Research B*, vol. 231, pp. 507–512, 2005.

[50] P. E. Dodd, M. R. Shaneyfelt, K. M. Horn et al., "SEU-sensitive volumes in bulk and SOI SRAMs from first-principles calculations and experiments," *IEEE Transactions on Nuclear Science*, vol. 48, no. 6, pp. 1893–1903, 2001.

[51] G. Vizkelethy, P. E. Dodd, J. R. Schwank et al., "Anomalous charge collection from silicon-on-insulator structures," *Nuclear Instruments and Methods in Physics Research B*, vol. 210, pp. 211–215, 2003.

[52] V. Ferlet-Cavrois, P. Paillet, J. R. Schwank et al., "Charge collection by capacitive influence through isolation oxides," *IEEE Transactions on Nuclear Science*, vol. 50, no. 6, pp. 2208–2218, 2003.

[53] G. Vizkelethy, D. K. Brice, and B. L. Doyle, "The theory of ion beam induced charge in metal-oxide-semiconductor structures," *Journal of Applied Physics*, vol. 101, no. 7, Article ID 074506, 6 pages, 2007.

[54] A. D. C. Alves, S. Thompson, C. Yang, and D. N. Jamieson, "Mapping ion beam induced current changes in a commercial MOSFET," *Nuclear Instruments and Methods in Physics Research B*, vol. 269, pp. 2355–2359, 2011.

[55] C. Donolato, R. Nipoti, D. Govoni, G. P. Egeni, V. Rudello, and P. Rossi, "Images of grain boundaries in polycrystalline silicon solar cells by electron and ion beam induced charge collection," *Materials Science and Engineering B*, vol. 42, no. 1–3, pp. 306–310, 1996.

[56] C. Donolato and R. Nipoti, "Simulation of pulse height spectra in ion beam induced charge microscopy of polycrystalline silicon," *Journal of Applied Physics*, vol. 82, no. 2, pp. 742–747, 1997.

[57] K. K. Lee and D. N. Jamieson, "Characterization of silicon polycrystalline solar cells at cryogenic temperatures with ion beam-induced charge," *Solar Energy Materials and Solar Cells*, vol. 94, no. 12, pp. 2405–2410, 2010.

[58] V. Borjanović, M. Jakšić, Z. Pastuović, B. Pivac, and E. Katz, "IBIC Studies of structural defect activity in different polycrystalline silicon material," *Vacuum*, vol. 71, pp. 117–122, 2003.

[59] V. Borjanović, M. Jakšić, Ž. Pastuović et al., "Defects in polycrystalline silicon studied by IBICC," *Solar Energy Materials & Solar Cells*, vol. 72, pp. 487–494, 2002.

[60] L. C. G. Witham, D. N. Jamieson, R. A. Bardos, and A. Saint, "Trace elements and charge recombination in polycrystalline photovoltaic materials," *Nuclear Instruments and Methods in Physics Research B*, vol. 136–38, pp. 1361–1365, 1998.

[61] A. M. Jakob, D. Spemann, R. Thies, J. Barzola-Quiqui, J. Vogt, and T. Butz, "A characterisation of electronic properties of alkaline texturized polycrystalline silicon solar cells using IBIC," *Nuclear Instruments and Methods in Physics Research B*, vol. 269, pp. 2345–2349, 2011.

[62] R. Hofstadter, "Remarks on diamond crystal counters," *Physical Review*, vol. 73, no. 6, p. 631, 1948.

[63] C. Canali, E. Gatti, S. F. Kozlov et al., "Electrical properties and performances of natural diamond nuclear radiation detectors," *Nuclear Instruments and Methods*, vol. 160, no. 1, pp. 73–77, 1979.

[64] E. A. Burgemeister, "Dosimetry with a diamond operating as a resistor," *Physics in Medicine and Biology*, vol. 25, pp. 519–532, 1981.

[65] D. R. Kania, M. I. Landstrass, M. A. Plano, L. S. Pan, and S. Han, "Diamond radiation detectors," *Diamond and Related Materials*, vol. 2, no. 5–7, pp. 1012–1019, 1993.

[66] C. Manfredotti, "CVD diamond detectors for nuclear and dosimetric applications," *Diamond and Related Materials*, vol. 14, pp. 531–540, 2005.

[67] C. Manfredotti, F. Fizzotti, E. Vittone, S. Bistolfi, M. Boero, and P. Polesello, "Grain size effects in CVD diamond detectors," *Nuclear Instruments and Methods in Physics Research B*, vol. 93, no. 4, pp. 516–520, 1994.

[68] C. Manfredotti, F. Fizzotti, E. Vittone et al., "IBIC investigations on CVD diamond," *Nuclear Instruments and Methods in Physics Research B*, vol. 100, no. 1, pp. 133–140, 1995.

[69] M. Jakšić, T. Tadić, I. Orlić, T. Osipowicz, E. Vittone, and C. Manfredotti, "Imaging of charge collection properties of CVD diamond using high-resolution ion beam induced charge technique with protons and alpha particles," *New Diamond and Frontier Carbon Technology*, vol. 8, no. 5, pp. 391–398, 1998.

[70] C. Manfredotti, F. Fizzotti, A. LoGiudice et al., "Ion microbeam analysis of CVD diamond," *Diamond and Related Materials*, vol. 8, no. 8-9, pp. 1597–1601, 1999.

[71] P. J. Sellin, A. Lohstroh, A. W. Davies et al., "Charge transport in polycrystalline and single crystal synthetic diamond using ion beam induced charge imaging," *Nuclear Instruments and Methods in Physics Research B*, vol. 260, no. 1, pp. 293–298, 2007.

[72] L. Milazzo and A. Mainwood, "Modelling of diamond detectors: effects of the polycrystalline structure and a pulse shape analysis," *Diamond and Related Materials*, vol. 13, no. 4–8, pp. 934–937, 2004.

[73] S. M. Hearne, D. N. Jamieson, E. Trajkov, S. Prawer, and J. E. Butler, "Temperature-dependent emptying of grain-boundary charge traps in chemical vapor deposited diamond," *Applied Physics Letters*, vol. 84, no. 22, pp. 4493–4495, 2004.

[74] C. Manfredotti, E. Vittone, C. Paolini, P. Olivero, and A. Lo Giudice, "Blue light sensitization of CVD diamond detectors," *Diamond and Related Materials*, vol. 12, no. 3–7, pp. 662–666, 2003.

[75] C. Manfredotti, F. Fizzotti, P. Polesello et al., "IBIC and IBIL microscopy applied to advanced semiconductor materials," *Nuclear Instruments and Methods in Physics Research B*, vol. 136–138, pp. 1333–1339, 1998.

[76] M. B. H. Breese, P. J. Sellin, L. C. Alves, A. P. Knights, R. S. Sussmann, and A. J. Whitehead, "Imaging of charge transport properties in polycrystalline CVD diamond using IBIC and IBIL microscopy," *Nuclear Instruments and Methods in Physics Research B*, vol. 181, no. 1–4, pp. 219–224, 2001.

[77] H. Pernegger, S. Roe, P. Weilhammer et al., "Charge-carrier properties in synthetic single-crystal diamond measured with the transient-current technique," *Journal of Applied Physics*, vol. 97, Article ID 073704, 9 pages, 2005.

[78] C. Manfredotti, F. Fizzotti, K. Mirri et al., "A micro-IBIC comparison between natural and CVD diamond," *Diamond and Related Materials*, vol. 6, no. 2–4, pp. 320–324, 1997.

[79] C. Manfredotti, F. Fizzotti, P. Polesello, and E. Vittone, "IBIC investigation of radiation-induced effects in CVD and natural diamond," *Nuclear Instruments and Methods in Physics Research A*, vol. 426, no. 1, pp. 156–163, 1999.

[80] A. Lohstroh, P. J. Sellin, S. Gkoumas et al., "Ion beam induced charge (IBIC) irradiation damage study in synthetic single crystal diamond using 2.6 MeV protons," *Physica Status Solidi*, vol. 205, no. 9, pp. 2211–2215, 2008.

[81] A. Lohstroh, P. J. Sellin, S. G. Wang et al., "Effect of dislocations on charge carrier mobility-lifetime product in synthetic single crystal diamond," *Applied Physics Letters*, vol. 90, no. 10, Article ID 102111, 3 pages, 2007.

[82] D. Asner and CERN-RD42 collaboration, "Nuclear instruments and methods in physics research," *Diamond Pixel Modules*, vol. 636, no. S125, S129 pages, 2011.

[83] A. Lo Giudice, P. Olivero, C. Manfredotti et al., "Lateral IBIC characterization of single crystal synthetic diamond detectors," *Physica Status Solidi*, vol. 5, no. 2, pp. 80–82, 2011.

[84] F. Nava, G. Bertuccio, A. Cavallini, and E. Vittone, "Silicon carbide and its use as a radiation detector material," *Measurement Science and Technology*, vol. 19, no. 10, Article ID 102001, 2008.

[85] C. Manfredotti, F. Fizzotti, A. Lo Giudice, C. Paolini, E. Vittone, and F. Nava, "Investigation of 4H-SiC Schottky diodes by ion beam induced charge (IBIC) technique," *Applied Surface Science*, vol. 184, no. 1–4, pp. 448–454, 2001.

[86] A. L. Giudice, F. Fizzotti, C. Manfredotti, E. Vittone, and F. Nava, "Average energy dissipated by mega-electron-volt hydrogen and helium ions per electron-hole pair generation in 4H-SiC," *Applied Physics Letters*, vol. 87, no. 22, Article ID 222105, pp. 1–3, 2005.

[87] M. Jakšić, Z. Bosnjak, D. Gracin et al., "Characterisation of SiC by IBIC and other IBA techniques," *Nuclear Instruments and Methods in Physics Research B*, vol. 188, no. 1–4, pp. 130–134, 2002.

[88] A. L. Giudice, Y. Garino, C. Manfredotti, V. Rigato, and E. Vittone, "Angle resolved IBIC analysis of 4H-SiC Schottky diodes," *Nuclear Instruments and Methods in Physics Research B*, vol. 249, no. 1-2, pp. 213–216, 2006.

[89] K. K. Lee, T. Nishijima, T. Ohshima, and D. N. Jamieson, "Ion beam induced charge gate rupture of oxide on 6H-SiC," *Nuclear Instruments and Methods in Physics Research B*, vol. 181, no. 1–4, pp. 324–328, 2001.

[90] E. Vittone, V. Rigato, P. Olivero et al., "Temperature dependent IBIC study of 4H-SiC Schottky diodes," *Nuclear Instruments and Methods in Physics Research B*, vol. 231, no. 1–4, pp. 491–496, 2005.

[91] S. del Sordo, L. Abbene, E. Caroli, A. M. Mancini, A. Zappettini, and P. Ubertini, "Progress in the development of CdTe and CdZnTe semiconductor radiation detectors for astrophysical and medical applications," *Sensors*, vol. 9, no. 5, pp. 3491–3526, 2009.

[92] P. J. Sellin, A. W. Davies, S. Gkoumas et al., "Ion beam induced charge imaging of charge transport in CdTe and CdZnTe," *Nuclear Instruments and Methods in Physics Research B*, vol. 266, no. 8, pp. 1300–1306, 2008.

[93] Ž. Pastuović, M. Jakšić, R. B. James, K. Chattopadhyay, X. Ma, and A. Burger, "Influence of electrical contacts on charge collection profiles in CdZnTe studied by IBIC," *Nuclear Instruments and Methods in Physics Research A*, vol. 458, no. 1-2, pp. 254–261, 2001.

[94] C. Manfredotti, F. Fizzotti, P. Polesello et al., "Investigation on the electric field profile in CdTe by ion beam induced current," *Nuclear Instruments and Methods in Physics Research A*, vol. 380, no. 1-2, pp. 136–140, 1996.

[95] E. Vittone, F. Fizzotti, A. Lo Giudice, P. Polesello, and C. Manfredotti, "Simulation of a CdTe gamma ray detector based on collection efficiency profiles as determined by lateral IBIC," *Nuclear Instruments and Methods in Physics Research A*, vol. 428, no. 1, pp. 81–87, 1999.

[96] G. Vizkelethy, B. A. Brunett, D. S. Walsh, R. B. James, and B. L. Doyle, "Investigation of the electronic properties of Cadmium Zinc Telluride (CZT) detectors using a nuclear microprobe," *Nuclear Instruments and Methods in Physics Research A*, vol. 458, no. 1-2, pp. 563–567, 2001.

[97] Z. Medunic, M. Jakšić, Z. Z. Pastuović, and N. Skukan, "Temperature dependent TRIBIC in CZT detectors," *Nuclear Instruments and Methods in Physics Research B*, vol. 210, pp. 237–242, 2003.

[98] Z. Medunic, Z. Pastuović, M. Jakšić, and N. Skukan, "Studying of trap levels by the use of focused ion beams," *Nuclear Instruments and Methods in Physics Research B*, vol. 231, pp. 486–490, 2005.

[99] A. Bosio, N. Romeo, S. Mazzamuto, and V. Canevari, "Polycrystalline CdTe thin films for photovoltaic applications," *Progress in Crystal Growth and Characterization of Materials*, vol. 52, no. 4, pp. 247–279, 2006.

[100] N. Baier, A. Brambilla, G. Feuillet, A. Lohstroh, S. Renet, and P. Sellin, "EBIC and IBIC Imaging on Polycrystalline CdTe," *Nuclear Instruments and Methods in Physics Research A*, vol. 576, no. 1, pp. 5–9, 2007.

[101] E. Colombo, A. Bosio, S. Calusi et al., "IBIC analysis of CdTe/CdS solar cells," *Nuclear Instruments and Methods in Physics Research B*, vol. 267, no. 12-13, pp. 2181–2184, 2009.

[102] T. Nishijima, H. Sekiguchi, S. Matsuda et al., "Study of basic mechanisms of single event upset in low-capacitance Si and GaAs diodes using high-energy microbeams," *Nuclear Instruments and Methods in Physics Research B*, vol. 104, no. 1–4, pp. 528–532, 1995.

[103] T. Nishijima, H. Sekiguchi, S. Matsuda, and N. Shiono, "Research of Si and GaAs diode structures by Ion Beam Induced Charge (IBIC) collection," *Nuclear Instruments and Methods in Physics Research B*, vol. 130, no. 1–4, pp. 557–563, 1997.

[104] F. Nava, P. Vanni, C. Canali et al., "Analysis of Uniformity of as Prepared and Irradiated S.I. GaAs Radiation Detectors," *IEEE Transaction on Nuclear Science*, vol. 45, no. 3, pp. 609–616, 1998.

[105] E. Vittone, F. Fizzotti, K. Mirri et al., "IBIC analysis of gallium arsenide Schottky diodes," *Nuclear Instruments and Methods in Physics Research B*, vol. 158, no. 1, pp. 470–475, 1999.

[106] E. Vittone, P. Olivero, F. Nava et al., "Lateral IBIC analysis of GaAs Schottky diodes," *Nuclear Instruments and Methods in Physics Research B*, vol. 231, no. 1–4, pp. 513–517, 2005.

[107] C. Yang, A. Bettiol, D. Jamieson et al., "Investigation of light emitting diodes using nuclear microprobes," *Nuclear Instruments and Methods in Physics Research B*, vol. 158, no. 1, pp. 481–486, 1999.

[108] M. Jakšić, Ž. Pastuović, and T. Tadić, "New developments in IBIC for the study of charge transport properties of radiation detector materials," *Nuclear Instruments and Methods in Physics Research B*, vol. 158, pp. 458–463, 1999.

[109] Z. Pastuović, E. Vittone, I. Capan, and M. Jakšic, "Probability of divacancy trap production in silicon diodes exposed to focused ion beam irradiation," *Applied Physics Letters*, vol. 98, Article ID 092101, 3 pages, 2011.

[110] IAEA, "Utilization of ion accelerators for studying and modelling of radiation induced defects in semiconductors and insulators," F12024 Coordinated Research Programme 2012–2016, http://www-crp.iaea.org/html/rifa-show-activecrp.asp.

[111] M. Jakšić, Z. Medunić, M. Bogovac, and N. Skukan, "Radiation damage microstructures in silicon and application in position sensitive charged particle detection," *Nuclear Instruments and Methods in Physics Research B*, vol. 231, no. 1–4, pp. 502–506, 2005.

[112] G. Pellegrini, P. Roy, R. Bates et al., "Technology development of 3D detectors for high-energy physics and imaging," *Nuclear Instruments and Methods in Physics Research A*, vol. 487, no. 1-2, pp. 19–26, 2002.

[113] CERN RD50 Collaboration, "Radiation hard semiconductor devices for very high luminosity colliders," http://rd50.web.cern.ch/rd50/.

[114] P. Olivero, J. Forneris, M. Jakšic et al., "Focused ion beam fabrication and IBIC characterization of a diamond detector with buried electrodes," *Nuclear Instruments and Methods in Physics Research B*, vol. 269, pp. 2340–2344, 2011.

[115] L. M. Jong, J. N. Newnham, C. Yangg et al., "Charge sharing in multi-electrode devices for deterministic doping studied by IBIC," *Nuclear Instruments and Methods in Physics Research B*, vol. 269, pp. 2336–2339, 2011.

[116] J. Forneris, D. N. Jamieson, G. Giacomini, C. Yang, and E. Vittone, "Modeling of ion beam induced charge sharing experiments for the design of high resolution position sensitive detectors," *Nuclear Instruments and Methods in Physics Research B*.In press.